Letter

Densification of a polymer glass under high-pressure shear flow

Owen Brazil,[1] H. Özgür Özer,[2] Benjamin Watts,[3] John B. Pethica,[1] and Graham L. W. Cross[1,4,*]

[1]*School of Physics, CRANN & AMBER, Trinity College, Dublin D02 PN40, Ireland*

[2]*Department of Physics Engineering, Istanbul Technical University, 34469, Maslak, Sariyer, Istanbul, Turkey*

[3]*Laboratory for Synchrotron Radiation-Condensed Matter, Paul Scherrer Institute, 5232 Villigen, Switzerland*

[4]*Adama Innovations LLC, CRANN, Trinity College, Dublin 2, Ireland*

(Received 20 April 2021; revised 8 June 2022; accepted 14 July 2022; published 26 August 2022)

The properties of glasses can change significantly as they evolve toward equilibrium. Mechanical deformation appears to influence this physical aging process in conflicting ways, with experiments and simulations showing both effects associated with rejuvenation away from and overaging toward the equilibrium state. Here we report a significant densification effect in a polymer undergoing shear flow under high pressure. We used the high-aspect ratio geometry of the layer compression test to measure the uniform and homogeneous accumulation of plastic strain during isothermal confined compression of a deeply quenched film of polystyrene glass. Combined scanning transmission x-ray microscopy (STXM) and atomic force microscopy confirmed defect-free deformation leaving up to 1.2% residual densification under conditions of confined uniaxial strain. At higher peak strain, plastic shear flow extruded glass from below the compressing punch under conditions of a high background pressure. A further density increase of 2% was observed by STXM for a highly thinned residual thickness of polymer that nevertheless showed no signs of crystallization or internal strain localization. While the confined uniaxial densification can be accounted for by a simple elastic–plastic constitutive model, the high-pressure extrusion densification cannot.

DOI: 10.1103/PhysRevB.106.L060103

The microscopic processes underpinning plasticity in crystalline systems such as metals are well established [1]; however, much less is known about the physics of plastically deforming nonequilibrium systems such as long-chained glassy polymers [2,3]. Many of the properties of these materials such as mass density, mechanical strength, and segmental mobility are observed to evolve in time in a structural recovery process wherein the nonergodic system tends toward a more thermodynamically favorable configuration, generally shedding free volume in the process. Originally considered simply to accelerate [4] or reverse [5] intrinsic structural relaxation of disordered materials, mechanical deformation has eventually revealed itself to have more subtle effects on the evolution of nonequilibrium matter [6,7]. Indeed, a diverse range of mechanical effects on parameters connected to aging have been observed: Both small deformation [8,9] and fully yielded conditions [10] report effects such as orders of magnitude decrease in relaxation times during active flow [11,12] and mechanical erasure of physical aging [6]. As opposed to an effect simply confined along an axis of unstressed, thermal aging [6], it has been suggested that a polyamorphic transition may more appropriately capture the nature of inelastic deformation. Nevertheless the influence of plastic deformation on glassy polymer dynamics and structure remains unclear [3], with particular uncertainty in the role of compressive stress and strain [13].

While free volume has been somewhat deprecated as a structure–property predictor for—e.g., yield strength [14]—hydrostatic stress has been shown to have a profound effect on, for example, deep-notch conditioning of metallic glass [15,16] in keeping with Spaepen's picture of local shear rearrangements competing against space available for diffusion [17]. A particularly striking recent finding was the improvement to bulk metallic glass (BMG) ductility observed under combined shear and high positive hydrostatic pressure of compressive deep-notch loading, which showed shear band suppression, lower hardness, and higher enthalpy of a nominally rejuvenated state [18]. Conversely, of a small number of studies reported, compression may densify polymer glass: Stable compactification was found during cold-rolling with large plastic strain [19–21], and in plastic [22] and even preyield [23] unconfined uniaxial compression.

In this work we examine the residual density of a deeply quenched polymer glass thin film under combined shear and compressive hydrostatic high-stress conditions experiencing yield and then shear flow. In apparent contrast to the deep-notch BMG compression experiments, we see no effect on polymer density not explainable by residual elastic stress left by our test until shear flow ensues. At this point, a 2% densification is observed inconsistent with simple elastic–plastic mechanics and indicating a striking overaging effect. We report that yield alone during homogeneous confined compression of microscopic polymer films alters the density only as expected from elastic effects; however, severe plastic strain realized after releasing the confinement leads to compactification—i.e., densification

*crossg@tcd.ie

not explainable by volume-preserving plasticity and/or elastic effects.

Macroscopic sample scale experiments of glass deformation may suffer from unobservable internal strain localization defects of shear banding, crazing, and/or necking phenomena characterized by extreme strain inhomogeneity due to strain softening [24] and/or self-heating [25] that can mask more fundamental underlying plastic mechanisms. Our approach avoids this by testing microscopic, confined volumes of polymer where such limitations may be overcome while still avoiding mechanical size effects reported for the extreme sub-100-nm regime [26–28]: Isothermal conditions are easily maintained to prevent strain localization from self-heating, even at high strain rates [25], while confinement preserves the geometry of deformation of systems too small to monitor via optical microscopy. Unlike macroscopic-scale experimental studies, our experiments provide unambiguous evidence of homogeneous deformation of the amorphous state without strain localization or crystallization through combined scanning x-ray microscopy and atomic force microscopy (AFM) imaging.

Our experiment, which we call the layer compression test, goes as follows: A cylindrical, diamond flat punch tip of diameter $2a = 2140$ nm is indented into a precisely aligned ($< 0.15^\circ$) atactic polystyrene (1.13-MDa molecular weight) film of initial thickness $h_0 = 203$ nm, which is supported on a silicon $\langle 100 \rangle$ substrate with a 190-nm-thick Si_3N_4 CVD-grown coating (see Supplemental Material [29] for further sample preparation details). With a film thickness of $\sim 30\ R_g$ of our polymer, we do not expect mechanical size effects in our film [27,30]. The resultant, highly uniform deformation allows measured load L versus displacement h to be directly converted to a representative engineering stress $\sigma_{zz} = L/\pi a^2$ versus strain $\varepsilon_{zz} = h/h_0$ experienced throughout the compressed film region. Indentation is performed at a constant stress rate of 0.2 GPa/s with an MTS Dynamic Contact Module nanoindenter. We have recently shown that this confined compression testing geometry, shown as an insert in Fig. 1(a), results in uniform longitudinal uniaxial strain well past the point of first plastic yield [31,32]. Figure 1(a) plots indentation stress versus strain curves for four individual indents to different peak stresses into the atactic polystyrene (aPS) film. In the initial elastic regime, stress and strain are related as $\sigma_{zz} = M\varepsilon_{zz}$, where M is the confined elastic modulus, which is larger than Young's modulus for positive values of Poisson's ratio ν. The orange curve loaded to a peak stress $\sigma_{zz} = 0.14$ GPa within this regime shows minimal residual strain upon unloading. While subtle, the presence of the kink at Y_c separating elastic from inelastic deformation has been carefully studied, with the absence of plastic strain confirmed by careful analysis by AFM, confirming no residual surface disturbance to < 1 nm [24]. The apparent small hysteresis in the orange curve is due to residual thermal drift within the nanoindenter displacement sensor, while the upward curvature at very small strain is due to slight misalignment of the flat punch face to the polymer surface. Plastic yield occurs at an elevated confined yield stress $Y_c \approx 0.32$ GPa, which—in a linear elastic–plastic formulation—is related to the von Mises tensile yield stress Y_0 as $Y_c = (\frac{1-\nu}{1-2\nu})Y_0$. Beyond yield, stress versus strain retains a well-defined relationship: For a perfectly plastic material,

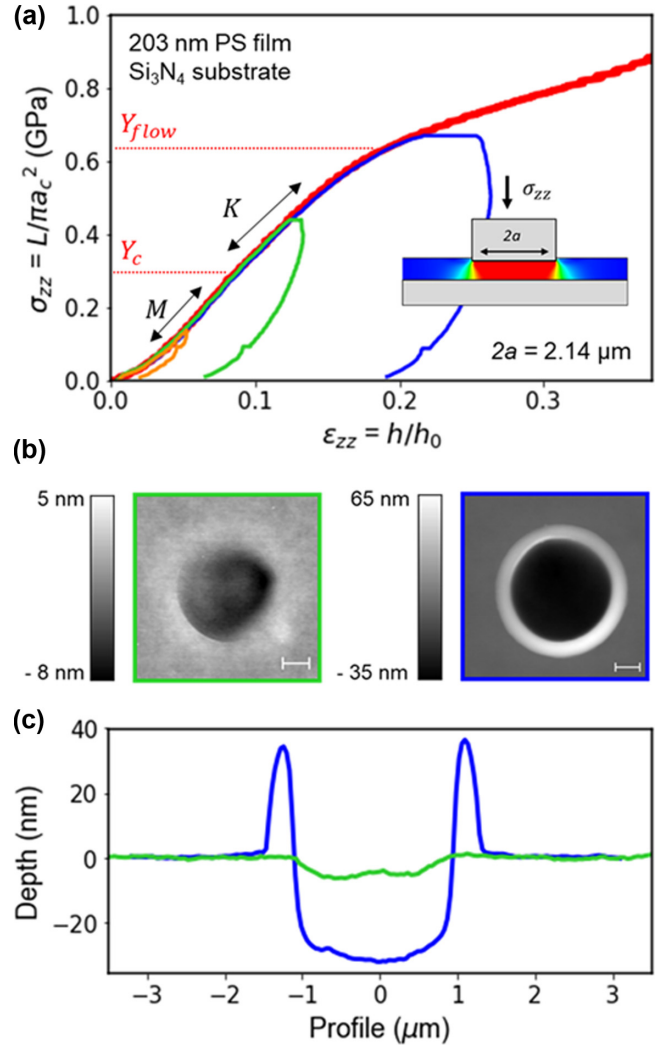

FIG. 1. Stress versus strain for a 203-nm aPS film indented via the layer compression test. Linear segments with slopes corresponding to elastic confined modulus M and bulk modulus K meet at the confined plastic yield point Y_c. (b) AFM images of residual deformation left in film by $\sigma_{zz} = 0.44-$GPa (green) and $\sigma_{zz} = 0.67-$GPa (blue) indents. (c) Accompanying height profiles extracted left to right from (b).

$\sigma_{zz} = K\varepsilon_{zz}$, where K is the bulk modulus. This results in a subtle slope change and the development of a significant residual strain of approximately 0.06, or 12 nm, upon unloading for the green curve in Fig. 1(a), loaded to a peak stress of 0.44 GPa. In Fig. 1(a), we can see that the layer compression test follows confined uniaxial compressive strain behavior in polystyrene up to about twice the confined yield strain [31] at $Y_{\text{flow}} = 0.65$ GPa, beyond which it diverges, as material beneath the punch starts to extrude and flow laterally from beneath the punch, resulting in a second change in slope.

In the confined plastic regime, volume-preserving lateral flow is suppressed, which results in a one-dimensional densification process. This is demonstrated explicitly in Fig. 1(b) and (c), which shows AFM topography maps and height profiles of the residual deformation left in the film for the $\sigma_{zz} = 0.44-$GPa indent (green) loaded into the confined plastic

zone and the $\sigma_{zz} = 0.67-$GPa indent (blue) into the extrusion regime. In the case of the confined plastic indent, no pileup is present around the circular residual impression in Fig. 1(b), while the height profile in Fig. 1(c) shows a distinct net loss in volume. For the indent loaded to the extrusion regime, lateral flow is recovered as confinement fails, resulting in considerable pileup distributed roughly symmetrically around the indent and a far deeper residual impression. In many disordered material systems like bulk metallic glasses, polymers, and network glasses, densification has been observed to occur under severe plastic deformation. For example, silica glasses have demonstrated density increases approaching 20% following indentation with Berkovich tips [33]. However, two problems present themselves when attempting to quantify densification of amorphous systems experimentally at the microscale: First, the nonuniformity of subsurface deformation fields typical to indentation studies performed with complex tip geometries such as those mentioned earlier make it difficult to separate fundamental plastic compactification arising from shear catalyzed molecular or microstructural reordering from the more mundane effects of residual elastic pinning stresses that also prevent shape recovery [34]. Second, there is the significant issue of accurately measuring mass density for nanometer-scale volumes. A commonly employed approach is to measure the volume of displaced material present in the pileup via AFM and compare this to the "missing" material volume in the residual indent impression, attributing any discrepancy to densification (or rejuvenation, in the case of greater pileup) [35]. As AFM is purely a surface metrology technique, however, a weakness arises in this approach in that it does not allow for subsurface localization effects such as shear banding or, in the case of a film on a substrate, delamination. Here, we overcome both of these difficulties with the aid of an additional experimental technique, scanning transmission x-ray microscopy (STXM), and gain a greater understanding of the degree of densification that occurs in polymer glasses through shear stress–induced reordering.

The flat punch indentation of a thin polymer film closely approximates confined uniaxial strain compression, which enables residual stresses and the resultant elastic densification to be determined analytically [31,32]. For a linear elastic–perfectly plastic material loaded to a peak stress $\sigma_p > Y_c$, the residual strain on unload is

$$\varepsilon_{\text{res}} = \left(\frac{Y_c - \sigma_p}{M}\right) + \left(\frac{\sigma_p - Y_c}{K}\right), \tag{1}$$

and in the absence of constitutive effects beyond a simple elastic–plastic model, the relative density increase is (see Supplemental Material [29]):

$$\rho/\rho_0 = 1/(1 - \varepsilon_{\text{res}}). \tag{2}$$

Finite element simulations of the confined compression of an elastic–plastic material (see Supplemental Material [29]) confirm the validity of this equation, therefore enabling volume changes resulting from elastic pinning through residual stresses to be subtracted from the total densification. Despite the somewhat idealized nature of this linear elastic–plastic model when applied to glassy polymers, we have shown it to be extremely effective in describing the complex stresses and strains these materials are subjected to in confined compression—in particular, the residual stress state upon unloading [32]. For the density measurement problem, we employ a unique approach based on a combination of AFM film thickness measurements and STXM to measure the relative mass density of the indented region through the bulk of the film without reference to the pileup surrounding the residual impression.

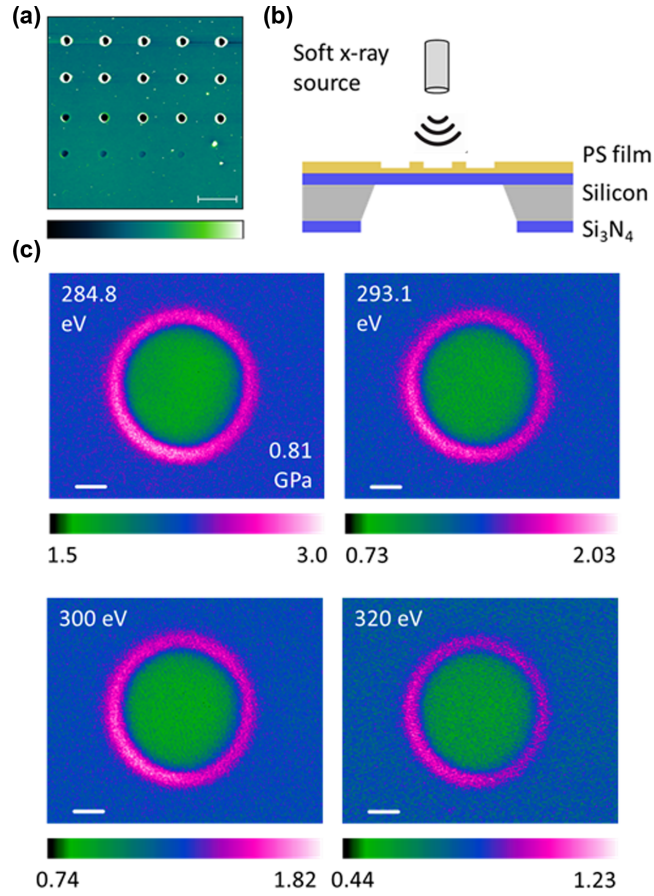

FIG. 2. (a) AFM topography map of indent array. (b) Sketch of x-ray transparent indented film sample for STXM measurement. (c) STXM optical density maps for layer compression indent to $\sigma_{zz} =$ 0.81 GPa taken at four beam energies.

STXM measurements were performed at the PolLux end station [36–38] at the Swiss Light Source synchrotron, Villigen, Switzerland. As a transmission-based technique, this allows direct confirmation of deformation homogeneity, ruling out shear banding and subsurface strain localization effects [39] not associated with fundamental molecular-scale plasticity in the polymer. Layer compression indentation was performed into the 203-nm aPS film so as to produce an array of indents spanning a peak stress array of 0.1 to 0.84 GPa, covering the confined elastic, confined plastic, and post-confinement extrusion regime. An AFM topography map of the indent array is shown in Fig 2(a). As was observed in Fig. 1, the recorded indentation stress–strain curves are highly repeatable and are used to extract the film mechanical parameters. With the top side of the film protected, the sample was back-etched in a 5-M NaOH solution at 55 °C for approximately two days to remove the silicon beneath

the array, leaving only the aPS film and an x-ray transparent supporting Si_3N_4 window. A sketch of this sample geometry is shown in Fig. 2(b). STXM measurements were carried out on each indent, primarily at a beam energy of 284.8 eV, corresponding to the $1s \rightarrow 1\pi * \text{C}=\text{C}$ molecular orbital transition in the polystyrene phenyl ring, where x-ray absorption is strongest and thus provides a maximum signal [40]. Using Beer-Lambert absorption laws, this x-ray transmission map was converted to an optical density map, from which the calculated Si_3N_4 background [41] was subtracted to isolate the optical density map of only the polymer in the indented region. An optical density map for an indent to a peak stress of 0.81 GPa—well into the extrusion regime—is shown in Fig. 2(c). No evidence of strain localization phenomena is observed, with the deformed region appearing homogeneous. By performing measurements at additional side group (300 eV, $1s \rightarrow 1\sigma * \text{C}=\text{C}$) and backbone (293.1 eV, $1s \rightarrow 1\sigma * \text{C}=\text{C}$) energies, whose optical density maps are also shown in Fig. 2(c), it may be seen that no linear dichroism effects are observable within the resolution of this technique [42], indicating a lack of molecular alignment and ordering within the observed film, and that the shear-driven densification remains amorphous. A nonresonant scan at $E = 320$ eV is included for comparison.

Relative mass density measurements are obtained via STXM in the manner previously described by Watts *et al.* [43]. Briefly, the initial thickness of the film was measured via profilometry across a film edge, and a topography map of the indented regions was obtained via AFM. This was converted to a thickness map [Fig. 3(a(i))] by adding the mean film thickness. The aPS optical density map measured via STXM and shown in Fig. 3(a(ii)) was converted to an absorption coefficient map by dividing by the AFM thickness map, then was further normalized to the average absorption coefficient in a $1-\mu\text{m}^2$ region far from any indentions as $A/A_0 = \rho/\rho_0$, where A_0 is the absorption coefficient in the nonindented region and ρ_0 is the typical nonindented film mass density. Since the absorption coefficient, A, of a material is proportional to its mass density, ρ, the normalized map [Fig. 3(a(iii))] shows variations in the mass density relative to the undeformed aPS film.

Relative density measurements, which have been spatially averaged across the entire compressed region, are plotted as a function of peak indentation stress in Fig. 3(b). Density contrast was measurable only for residual indentation craters made with a peak stress above 0.4 GPa, somewhat above the measured yield stress due to an insufficient signal-to-noise ratio at lower stresses. Examination of the relevant load–displacement curves and AFM measurements at the site of indentation for tests performed to peak stresses below Y_c indicated no residual deformation, however, allowing us to infer that no densification has occurred. The elastic–plastic relative densification generated through trapped residual stresses predicted by Eqs. (1) and (2) is plotted in blue using fitted layer compression test values of $M = 4.6$ GPa, $K = 3.8$ GPa, and $Y_c = 0.32$ GPa extracted from the stress-versus-strain data recorded during indentation. A curious feature of linear elastic–plastic mechanics in a confined uniaxial strain geometry such as that studied here is that the amount of residual shear stress the deformed volume is capable of storing has a well-defined and finite limit, which occurs at an applied stress of $\sigma_{zz} = 2Y_c$ [24]. Within this framework, the relative densification caused by these residual stresses in Eq. (2) should become capped and plateau at a value of 1.5% using the values of M, K, and Y_c we measure. Up to $2Y_c = 0.64$ GPa, the predicted linear increase in density with increasing σ_p shows excellent agreement with the values measured experimentally via STXM. Rather than plateauing at this point, however, the data continue to rise before leveling off at a slightly higher stress of 0.68 GPa. At a value of 0.81 GPa, the material below the punch fully extrudes. The residual material left in the deeper indentation crater has undergone further extensive densification to 3.4% or more, almost 2% higher than a simple elastic–plastic prediction for any confined state. With reference to the stress–strain curve of Fig. 1(a), we note the last two density measurements occur at stresses corresponding to extremely large representative indentation strains, approximately 30% for the $\sigma_{zz} = 0.81-$GPa indent.

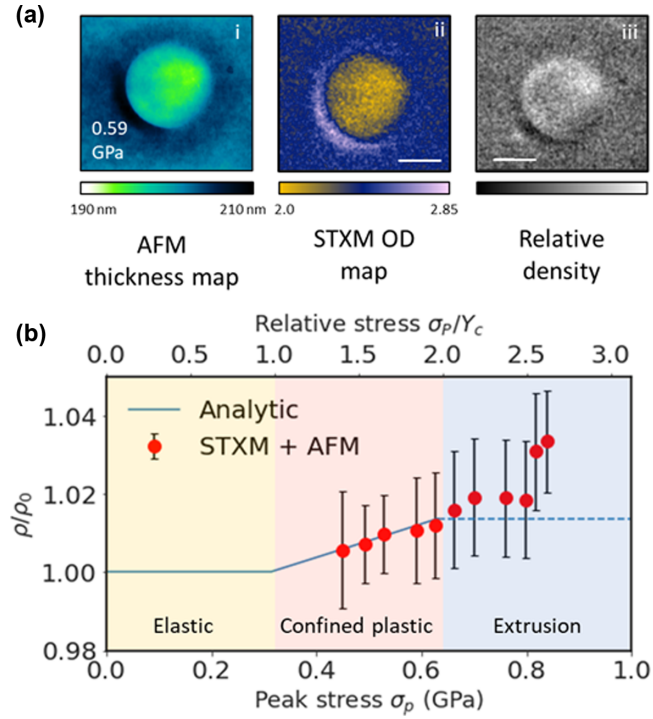

FIG. 3. (a) Method for determining relative permanent densification (iii) in polystyrene film-based AFM height maps (i) and STXM (ii) measurements. (b) Residual density increase for a 203-nm polystyrene film as a function of peak compressive stress σ_p in the layer compression test. Permanent densification up to 3.4% is observed under extrusive shear flow at high peak stress.

The x-ray measurements do not rely on assumptions about mass conservation in the compacted region, which would be required if surface topography change (e.g., via AFM surface imaging alone) was the measure of density. As a result, data can be obtained beyond confinement, where extrusion has occurred without concern over potential introduction of cavities by delamination beneath the extruded region [such features have occasionally been observed at the edge of indents in focused ion beam (FIB) cross sections]. From Fig. 1, we note that 0.65 GPa corresponds approximately

to the stress at which plastic failure of confinement takes place, beyond which extrusion significantly increases the amount of shear strain within the material. We observe that a permanent density increase continues beyond this point as well, in conflict with the simple confined compression (CC) elastic–plastic model prediction of Fig. 3(a), which indicates a strict limit to densification occurring at $2Y_c$ ($\sim$0.64 GPa). This further density increase behavior might be explained by a pressure-dependent yield surface, which would allow for more densification via the residual stress mechanism explained earlier by enabling additional shear loading during plasticity. However, our yield measurement shows that a pressure-dependent shift in yield strain is, at most, a 20% effect and therefore is unable to explain our data. Alternatively, segmental rearrangement to a denser glassy state may be taking place. The onset of extrusion results in greatly increased material transport and therefore must be accommodated by an increase in molecular mobility, which nevertheless occurs in a highly squeezed geometry between substrate and punch still subject to significant hydrostatic stress generated by σ_{zz}. In this deformation condition, new modes of shear-assisted segmental rearrangement may become available, where a net densification is favored over free-volume generation due to the applied compressive stress. Overall, we find large excess homogeneous densification of a polymer glass for a large shear strain under high pressure.

Our experiments demonstrate a previously unachieved level of precision with which to study the deformation processes occurring in small, confined polymer volumes, with well-defined levels of strain and allowance for stored elastic stresses. Further, the thinness of the sample implies a strict absence of any dissipative temperature increase within the polymer for the strain rates we have used. We find that in the presence of large hydrostatic pressure, shear flow compactifies polymer glass. The presence of some plastic strain under fully confined compression produces a density increase expected from conventional volume-preserving plastic mechanics with elasticity. However, further plastic strain and extrusion produces a substantial further density increase that cannot be so explained. While chain connectivity generally is thought to play only a minor role in nonequilibrium processes such as the glass transition and structural relaxation [3], one area where it is of critical importance is in plastic deformation under large strain, where the stability offered by the network enables ductile yield to occur. By contrast, bulk metallic glasses and low-molecular weight polymers are subject to strain softening and intense shear localization, leading to brittle fracture in most deformation geometries [44]. Indeed the nature of fundamental local rearrangements of atomic clusters carrying plasticity in recent atomistic simulation of polystyrene compression is found to be profoundly affected by chain connectivity [45].

Recent experiments in deep-notched or poker chip geometries similar to that consider here have shown that metallic glasses may demonstrate ductile yielding in both tension and compression due to a pressure-modulated molecular reordering mechanism that suppresses shear banding and results in increased density in longitudinal tension and reduced density in confined compression [15,16]. However, our results show that for high-molecular weight polymer glasses, the opposite is true; density increases in confined compression. Overall, we conclude that even under gigapascal-level hydrostatic pressures that inhibit large-scale molecular mobility, network and chain topology remain crucial in how disordered systems respond to plastic shear.

O.B., J.B.P., and G.L.W.C. acknowledge funding from the Science Foundation Ireland–funded AMBER research center (SFI/12/RC/2278). We acknowledge the Paul Scherrer Institut, Villigen, Switzerland for provision of synchrotron radiation beamtime at the PolLux beamline of the SLS. The PolLux end station was financed by the German Ministerium für Bildung und Forschung (BMBF) through Contracts No. 05K16WED and No. 05K19WE2.

[1] G. E. Dieter, *Mechanical Metallurgy*, 3rd ed. (McGraw-Hill, London, 1988).
[2] A. S. Argon, *The Physics of Deformation and Fracture of Polymers* (Cambridge University Press, Cambridge, 2013).
[3] C. B. Roth, *Polymer Glasses* (CRC Press, Boca Raton, 2016).
[4] F. A. Myers, F. C. Cama, and S. S. Sternstein, Mechanically enhanced aging of glassy polymers, Ann. N. Y. Acad. Sci. **279**, 94 (1976).
[5] L. C. E. Struik, On the rejuvenation of physically aged polymers by mechanical deformation, Polymer **38**, 4053 (1997).
[6] G. B. McKenna, Mechanical rejuvenation in polymer glasses: Fact or fallacy? J. Phys. Condens. Matter **15**, S737 (2003).
[7] T. Bennin, E. Xing, J. Ricci, and M. D. Ediger, Rejuvenation versus overaging: The effect of cyclic loading/unloading on the segmental dynamics of poly(methyl methacrylate) glasses, Macromolecules **53**, 8467 (2020).
[8] L. V. Pastukhov, M. J. W. Kanters, T. A. P. Engels, and L. E. Govaert, Physical background of the endurance limit in poly(ether ether ketone), J. Polym. Sci. A **58**, 716 (2020).
[9] C. C. W. J. Clarijs, M. J. W. Kanters, M. J. Erp, T. A. P. Engels, and L. E. Govaert, Predicting plasticity-controlled failure of glassy polymers: Influence of stress-accelerated progressive physical aging, J. Polym. Sci. B Polym. Phys. **57**, 1300 (2019).
[10] M. L. Wallace and B. Joós, Shear-Induced Overaging in a Polymer Glass, Phys. Rev. Lett. **96**, 025501 (2006).
[11] B. Bending, K. Christison, J. Ricci, and M. D. Ediger, Measurement of segmental mobility during constant strain rate deformation of a poly(methyl methacrylate) glass, Macromolecules **47**, 800 (2014).
[12] R. A. Riggleman, H.- N. Lee, M. D. Ediger, and J. J. de Pablo, Free Volume and Finite-Size Effects in a Polymer Glass Under Stress, Phys. Rev. Lett. **99**, 215501 (2007).
[13] J. M. Caruthers and G. A. Medvedev, in *Polymer Glasses*, 1st ed. (CRC Press, Boca Raton, 2016), pp. 106–178.
[14] D. Richard, M. Ozawa, S. Patinet, E. Stanifer, B. Shang, S. A. Ridout, B. Xu, G. Zhang, P. K. Morse, J.-L. Barrat, L. Berthier, M. L. Falk, P. Guan, A. J. Liu, K. Martens, S. Sastry, D. Vandembroucq, E. Lerner, and M. L. Manning, Predicting

plasticity in disordered solids from structural indicators, Phys. Rev. Materials **4**, 113609 (2020).

[15] J. Pan, Y. X. Wang, Q. Guo, D. Zhang, A. L. Greer, and Y. Li, Extreme rejuvenation and softening in a bulk metallic glass, Nat. Commun. **9**, 560 (2018).

[16] Z. T. Wang, J. Pan, Y. Li, and C. A. Schuh, Densification and Strain Hardening of a Metallic Glass Under Tension at Room Temperature, Phys. Rev. Lett. **111**, 135504 (2013).

[17] M. Heggen, F. Spaepen, and M. Feuerbacher, Creation and annihilation of free volume during homogeneous flow of a metallic glass, J. Appl. Phys. **97**, 033506 (2004).

[18] J. Pan, Y. P. Ivanov, W. H. Zhou, Y. Li, and A. L. Greer, Strain-hardening and suppression of shear-banding in rejuvenated bulk metallic glass, Nature (London) **578**, 559 (2020).

[19] L. J. Broutman and R. S. Patil, Cold rolling of polymers: 1. Influence of rolling on properties of amorphous polymer, Polym. Eng. Sci. **11**, 165 (1971).

[20] H. G. H. van Melick, L. E. Govaert, B. Raas, W. J. Nauta, and H. E. H. Meijer, Kinetics of ageing and re-embrittlement of mechanically rejuvenated polystyrene, Polymer **44**, 1171 (2003).

[21] D. Cangialosi, M. Wübbenhorst, H. Schut, A. van Veen, and S. J. Picken, Amorphous–amorphous transition in glassy polymers subjected to cold rolling studied by means of positron annihilation lifetime spectroscopy, J. Chem. Phys. **122**, 064702 (2005).

[22] L. Xie, D. W. Gidley, H. A. Hristov, and A. F. Yee, Evolution of nanometer voids in polycarbonate under mechanical stress and thermal expansion using positron spectroscopy, J. Polym. Sci. B Polym. Phys. **33**, 77 (1995).

[23] D. M. Colucci, P. A. O'Connell, and G. B. McKenna, Stress relaxation experiments in polycarbonate: A comparison of volume changes for two commercial grades, Polym. Eng. Sci. **37**, 1469 (1997).

[24] H. G. H. van Melick, L. E. Govaert, and H. E. H. Meijer, Localisation phenomena in glassy polymers: Influence of thermal and mechanical history, Polymer **44**, 3579 (2003).

[25] G. M. Swallowe, in *Adiabatic Shear Localization*, 2nd ed., edited by B. Dodd and Y. Bai (Elsevier, Oxford, 2012), pp. 363–398.

[26] M. Alcoutlabi and G. B. McKenna, Effects of confinement on material behaviour at the nanometre size scale, J. Phys. Condens. Matter **17**, R461 (2005).

[27] H. D. Rowland, W. P. King, J. B. Pethica, and G. L. W. Cross, Molecular confinement accelerates deformation of entangled polymers during squeeze flow, Science **322**, 720 (2008).

[28] L. Si, M. V. Massa, K. Dalnoki-Veress, H. R. Brown, and R. A. L. Jones, Chain Entanglement in Thin Freestanding Polymer Films, Phys. Rev. Lett. **94**, 127801 (2005).

[29] See Supplemental Material at http://link.aps.org/supplemental/10.1103/PhysRevB.106.L060103 for sample preparation details, derivation, and a description of finite element simulation.

[30] D. Nieto Simavilla, W. Huang, C. Housmans, M. Sferrazza, and S. Napolitano, Taming the strength of interfacial interactions via nanoconfinement, ACS Cent Sci **4**, 755 (2018).

[31] O. Brazil, J. P. de Silva, M. Chowdhury, H. Yoon, G. B. McKenna, W. C. Oliver, J. Kilpatrick, J. B. Pethica, and G. L. W. Cross, In situ measurement of bulk modulus and yield response of glassy thin films via confined layer compression, J. Mater. Res. **35**, 644 (2020).

[32] O. Brazil, J. P. de Silva, J. B. Pethica, and G. L. W. Cross, Extrinsic plastic hardening of polymer thin films in flat punch indentation, Philos. Mag. **101**, 1327 (2021).

[33] T. Rouxel, H. Ji, J. P. Guin, F. Augereau, and B. Rufflé, Indentation deformation mechanism in glass: Densification versus shear flow, J. Appl. Phys. **107**, 094903 (2010).

[34] D. Vandembroucq, T. Deschamps, C. Coussa, A. Perriot, E. Barthel, B. Champagnon, and C. Martinet, Density hardening plasticity and mechanical ageing of silica glass under pressure: A Raman spectroscopic study, J. Phys. Condens. Matter **20**, 485221 (2008).

[35] K. R. Gadelrab, F. A. Bonilla, and M. Chiesa, Densification modeling of fused silica under nanoindentation, J. Non-Cryst. Solids **358**, 392 (2012).

[36] J. Raabe1 *et al.*, PolLux: A new facility for soft x-ray spectromicroscopy at the Swiss light source, Rev. Sci. Instrum. **79**, 113704 (2008).

[37] U. Frommherz, J. Raabe, B. Watts, R. Stefani, and U. Ellenberger, Higher order suppressor (HOS) for the PolLux microspectroscope beamline at the Swiss light source SLS, in *10th International Conference on Radiation Instrumentation, SRI 2009*, edited by R. Garrett, I. Gentle, K. Nugent, and S. Wilkins, AIP Conf. Proc. No. 1234 (AIP, Melville, New York, 2010), p. 429.

[38] U. Flechsig, C. Quitmann, J. Raabe, M. Böge, R. Fink, and H. Ade, The PolLux microspectroscopy beam line at the Swiss light source, in *Synchrotron Radiation Instrumentation: Ninth International Conference on Synchrotron Radiation Instrumentation*, edited by J.-Y. Choi and S. Rah, AIP Conf. Proc. No. 879 (AIP, Melville, New York, 2007), p. 505.

[39] J. C. M. Li, Behavior and properties of shear bands, Polym. Eng. Sci. **24**, 750 (1984).

[40] O. Dhez, H. Ade, and S. G. Urquhart, Calibrated NEXAFS spectra of some common polymers, J. Electron Spectrosc. Relat. Phenom. **128**, 85 (2003).

[41] B. L. Henke, E. M. Gullikson, and J. C. Davis, X-ray interactions: Photoabsorption, scattering, transmission, and reflection at $E = 50$–$30,000$ EV, $Z = 1$–92, Atomic Data Nucl. Data Tables **54**, 181 (1993).

[42] B. Watts, T. Schuettfort, and C. R. McNeill, Mapping of domain orientation and molecular order in polycrystalline semiconducting polymer films with soft x-ray microscopy, Adv. Funct. Mater. **21**, 1122 (2011).

[43] B. Watts, P. Warnicke, N. Pilet, and J. Raabe, Nanoscale measurement of the absolute mass density of polymers: Nanoscale measurement of the absolute mass density of polymers, Phys. Status Solidi **212**, 518 (2015).

[44] J. Liu, P. Lin, S. Cheng, W. Wang, J. W. Mays, and S.- Q. Wang, Polystyrene glasses under compression: Ductile and brittle responses, ACS Macro Lett. **4**, 1072 (2015).

[45] R. H. M. Mols, G. G. Vogiatzis, L. C. A. van Breemen, and M. Hütter, Microscopic carriers of plasticity in glassy polystyrene, Macromol. Theory Simul., **30**, 2100021 (2021).